THE JOURNAL OF BIOLOGICAL CHEMISTRY Vol. 272, No. 23, Issue of June 6, pp. 14830–14841, 1997
Printed in U.S.A.

Architectural Accommodation in the Complex of Four p53 DNA Binding Domain Peptides with the *p21/waf1/cip1* DNA Response Element*

(Received for publication, January 10, 1997, and in revised form, March 25, 1997)

Akhilesh K. Nagaich‡, Victor B. Zhurkin§, Hiroshi Sakamoto¶, Andrey A. Gorin‖, G. Marius Clore, Angela M. Gronenborn**, Ettore Appella¶, and Rodney E. Harrington‡ ‡‡**

*From the ‡Department of Biochemistry/330, School of Medicine, University of Nevada Reno, Reno, Nevada 89557-0014, the ‖Department of Chemistry, Rutgers University, Piscataway, New Jersey 08855, the §Laboratory of Experimental and Computational Biology and ¶Laboratory of Cell Biology, NCI, National Institutes of Health, Bethesda, Maryland 20892, and the **Laboratory of Chemical Physics, NIDDK, National Institutes of Health, Bethesda, Maryland 20892*

High resolution chemical footprinting and cross-linking experiments have provided a basis for elucidating the overall architecture of the complex between the core DNA binding domain of p53 (p53DBD, amino acids 98–309) and the *p21/waf1/cip1* DNA response element implicated in the G_1/S phase cell cycle checkpoint. These studies complement both a crystal structure and earlier biophysical studies and provide the first direct experimental evidence that four subunits of p53DBD bind to the response element in a regular staggered array having pseudodyad symmetry. The invariant guanosines in the highly conserved C(A/T)|(T/A)G parts of the consensus half-sites are critical to the p53DBD-DNA binding. Molecular modeling of the complex using the observed peptide-DNA contacts shows that when four subunits of p53DBD bind the response element, the DNA has to bend ~50° to relieve steric clashes among different subunits, consistent with recent DNA cyclization studies. The overall lateral arrangement of the four p53 subunits with respect to the DNA loop comprises a novel nucleoprotein assembly that has not been reported previously in other complexes. We suggest that this kind of nucleoprotein superstructure may be important for p53 binding to response elements packed in chromatin and for subsequent transactivation of p53-mediated genes.

Wild type p53 is a widely distributed phosphoprotein that has become fundamental in cancer research (1–3). It functions as a tumor suppressor and is an essential component in the cell's response to DNA damage (4). It acts as a transcriptional enhancer for a number of DNA damage and growth arrest genes including *mdm2*, *gadd45*, and *p21/waf1/cip1*, the last being involved in the G_1/S phase checkpoint (5–8). When expressed at high levels, p53 suppresses transformation, arrests cells in G_1 phase, and in some cases promotes apoptosis (9–11). Studies of tumorigenic mutants have shown that the majority are selectively located at sites that map directly to the specific DNA binding domain of p53 (12). This fact, supported by recent biochemical and molecular genetic evidence, has clearly demonstrated that much of the biological function of p53 is mediated by its DNA binding properties (13, 14).

Wild type p53 binds over 100 different naturally occurring response elements, of which approximately 60 show functionality. It has been estimated that the human genome contains approximately 200–300 such sites (15). Response elements differ in details of specific base sequence, but all contain two tandem decameric elements, each a pentameric inverted repeat. Most decamers follow the consensus sequence pattern RRRC(A/T)|(A/T)GYYY, where R and Y are purines and pyrimidines, respectively, and the vertical bar denotes the center of dyad symmetry (16). These decameric elements may be separated by as much as 21 bp without complete loss of p53 binding affinity, but functional sites, defined as the ability to transcriptionally activate a nearby reporter gene, evidently follow very closely the consensus decamer pattern with no or only very short intervening spacers (15). Wild type p53 binds response elements through a sequence-specific DNA binding domain extending from amino acid residue 96 to 308 (13). Studies of tumor-derived p53 mutants have shown that they are defective in sequence-specific DNA binding and consequently cannot activate transcription (17). These studies have demonstrated that sequence-specific DNA binding and transactivation are the key biochemical activities responsible for much of the biological function of p53.

A recent cocrystal structure of a p53DBD[1] nucleoprotein complex has provided valuable insights into the binding specificity of p53 by identifying specific binding contacts (18). This important work has had a major impact on thinking about p53 structure-function relationships. However, both the complex size and the binding sequence were necessarily restricted in the cocrystal. Although the oligonucleotide used in the cocrystal contained a full 10-bp consensus half-site (Fig. 1*B*), only a single core domain peptide bound specifically with a consensus pentanucleotide, while a second bound nonspecifically 11 bp away and the third did not contact the DNA. Thus, many questions remain. These include the full origin of sequence specificity in DNA binding and the roles of specific p53 response elements, the multisubunit nature of the full p53 nucleoprotein complexes and the overall organization of p53 tetramers bound to the DNA recognition site, and the possible role of conformational changes in both the protein and the DNA as a consequence of complexation.

In the present study, we provide the first report of a struc-

* This work was supported by National Science Foundation Grant MCB 9117488, National Institutes of Health Grants HG00656 and CA70274, the U.S. Department of Agriculture Hatch Project NEV032D through the Nevada Experiment Station (to R. E. H.), and the AIDS Targeted Anti-Viral Program of the Office of the Director of the National Institutes of Health (to G. M. C., A. M. G., and E. A.). The costs of publication of this article were defrayed in part by the payment of page charges. This article must therefore be hereby marked "*advertisement*" in accordance with 18 U.S.C. Section 1734 solely to indicate this fact.

‡‡ To whom correspondence should be addressed.

[1] The abbreviations used are: p53DBD, p53 DNA binding domain; bp, base pair(s); MES, 4-morpholineethanesulfonic acid; bis-Tris, 2-[bis(2-hydroxyethyl)amino]-2-(hydroxymethyl)-propane-1,3-diol.

tural model for the complex of four human p53DBD peptides with an important functional response element: the *p21/waf1/cip1* binding site. This model goes considerably beyond that provided by the earlier crystallographic study and is able to rationalize a number of earlier observations including the requirement for DNA bending in the full tetrapeptide complex. It also provides unique insights into possible roles of DNA flexibility in the sequence specificity of p53 binding and suggests possible relationships between the relative orientation of a tetrameric p53 complex on response element DNA and p53 transactivational function.

The model is based on the results of several experiments sensitive to base-specific nucleoprotein contacts between the p53DBD peptides and response element DNA including hydroxyl radical footprinting, missing nucleoside analyses, and methylation and ethylation interference assays. Studies were conducted on a 65-bp oligonucleotide that includes the *p21/waf1/cip1* response element; this response element contains both a consensus (Fig. 1*A*, *boxes 1* and *2*) and a nonconsensus (*boxes 3* and *4*) half-site. To facilitate comparison of the present work with the crystallographically determined contact sites (18), we also studied a 67-bp oligonucleotide containing the same 20-bp binding sequence used in the cocrystal structure, designated in this work as the Cho sequence (Fig. 1*B*). Our solution results generally agree with the crystallographic contacts for the Cho sequence, although we find evidence for a second binding site of reverse orientation within this sequence that was not observed in the cocrystal. Our results for the *p21/waf1/cip1* site show unequivocally that four p53DBD peptides bind this response element in a staggered array and that each consensus pentanucleotide of the *p21/waf1/cip1* site makes specific contacts with the p53DBD and its invariant guanosine nucleotide playing a critical role. Hydroxyl radical footprinting demonstrates structural microheterogeneity in the consensus binding sites, suggesting that sequence-dependent structural variability of response elements plays a critical role in the binding of p53 with DNA. Model building of the p53DBD-*p21/waf1/cip1* nucleoprotein complex using the results of various chemical probes and footprinting shows that the four bound p53DBD peptides bend the response element by ~50° to relieve the steric clashes among the bound subunits. This model is in quantitative agreement with recent T4-DNA ligase-mediated cyclization studies (19) and with circular permutation gel retardation assays of the p53DBD-*p21/waf1/cip1* complex (20).

MATERIALS AND METHODS

Oligonucleotide Synthesis and Labeling—Oligonucleotides used in the study (Fig. 1), were synthesized and were purified on a 15% denaturing polyacrylamide gel. Equimolar amounts of complementary single-stranded oligonucleotides were mixed and annealed by heating to 90 °C and slowly cooling down to room temperature. Oligonucleotide duplexes, designed with one base overhang, were uniquely labeled at different ends of both strands. The top strands were labeled at the 3′-end with [α-^{32}P]dCTP using the Klenow fragment of DNA polymerase, and the bottom strand was labeled using [γ-^{32}P]ATP and polynucleotide kinase using standard procedures (21). The labeled duplexes were purified once more on 10% native polyacrylamide gels to remove traces of labeled single-stranded DNA and free [γ-^{32}P]ATP.

Preparation and Purification of the DNA Binding Domain of p53 (p53DBD)—A human p53 cDNA clone encoding amino acid residues 96–308 was amplified by polymerase chain reaction using p53-specific primers 5′-ATATCATATGGTCCCTTCCCAGAAAACCTA-3′ and 5′-ATATGGATCCTCACAGTGCTCGCTTAGTGCTC-3′. The amplified product was cloned in the pET12a expression vector (Novagen), and the core DNA binding domain was overproduced in *Escherichia coli* BL21 (DE3). The cells were incubated at 37 °C until an A_{600} of 0.6–1.0 was attained, and 0.25 mM isopropyl β-D-thiogalactoside was added to induce the expression of the recombinant protein. Cells were harvested after 2 h by centrifugation, lysed in a French press, and sonicated for 2 min in 40 mM MES, pH 6.0, 100 mM NaCl, 5 mM dithiothreitol. The soluble fraction was loaded onto a Resource S column (Pharmacia Biotech Inc.) in 40 mM MES, pH 6.0, 5 mM dithiothreitol and was eluted in a 0–400 mM NaCl gradient. The pooled fractions were precipitated by ammonium sulfate addition to 80% saturation and purified further on a Sephadex 75 HR gel filtration column (Pharmacia) in 50 mM bis-Tris propane-HCl, pH 6.8, 100 mM NaCl, 1 mM dithiothreitol. The purified p53DBD was checked on an SDS-polyacrylamide gel for purity.

Hydroxyl Radical Footprinting—Single end-labeled oligonucleotide duplexes (5×10^5 cpm, ~500 ng) were dissolved in a binding buffer containing 50 mM Tris-Cl, 10 mM dithiothreitol, and 50 mM NaCl (8 μl). Purified p53DBD (4 μg, ~1:14 DNA:protein molar ratio) was added and the complex was allowed to form for 30 min on ice. Hydroxyl radical cleavage reactions were initiated by adding a mixture containing 8 mM $FeS0_4(NH_4)_2SO_4{\cdot}6H_20$ and 16 mM EDTA (2 μl), 0.03% H_2O_2 (2 μl), and 20 mM sodium ascorbate (2 μl). Reactions were carried out on ice for 2 min and were quenched by adding 0.1 M thiourea (5 μl). Each sample was mixed with 15% Ficoll (4 μl) and was loaded on a 4% native polyacrylamide gel containing 20 mM HEPES, pH 8.3, as a running buffer. The gels were run for about 1 h at 8 V/cm to separate bound DNA from traces of unbound oligonucleotides. The bound fraction was gel-eluted in 0.5 M NH_4Cl, 0.1 mM EDTA, extracted with phenol:chloroform, precipitated twice with ethanol, and run out on a sequencing gel. The control DNA was also cleaved under identical conditions.

Missing Nucleoside Experiment—The labeled oligonucleotides (1×10^6 cpm, ~1 μg), dissolved in TE buffer, pH 7.6 (70 μl) were randomly gapped by reaction with hydroxyl radicals using a mixture of 1 mM $FeS0_4(NH_4)_2SO_4{\cdot}6H_2O$ and 2 mM EDTA (10 μl), 0.3% H_2O_2 (10 μl), and 10 mM sodium ascorbate (10 μl). The reactions were carried out on ice for 2 min and were quenched with 0.1 M thiourea (30 μl), 0.2 M EDTA (10 μl), 3 M sodium acetate (20 μl), and TE buffer (40 μl). The DNA was precipitated by adding 500 μl of ethanol. Each pellet was redissolved in 200 μl of 0.3 M sodium acetate containing 0.2 mM EDTA and was precipitated with 500 μl of ethanol. The pellet was washed with 70% ethanol, lyophilized, and dissolved in the binding buffer (18 μl). Purified p53DBD (5 μg) was added, and the complex was allowed to form for 30 min on ice. Each reaction was chased for 5 min with a 5 M excess of cold oligonucleotide duplexes to titrate any nonspecific complex formation. The amount of cold oligonucleotides and chasing time was adjusted such that 90% of DNA remained bound. The bound and unbound fractions were separated on a mobility shift gel, as described above, eluted from the gel, precipitated with ethanol, washed with 70% ethanol, and loaded on a sequencing gel. The control DNA was also cleaved under identical conditions.

Methylation Interference Assay—Labeled oligonucleotides (1×10^6 cpm, ~1 μg), were mixed in 200 μl of 50 mM sodium cacodylate, pH 8.0, 1 mM EDTA containing sonicated salmon sperm DNA (1 μg) and tRNA (2 μg) and were incubated with 0.5 μl of dimethyl sulfate at room temperature for 2 min. The methylation reactions were terminated by adding 50 μl of 1.5 M sodium acetate, 1 M β-mercaptoethanol, 100 μg/ml tRNA and 750 μl of ethanol. The DNA was precipitated twice with ethanol, dissolved in 50 μl of 0.4 M NaCl and reprecipitated with 1 ml of ethanol. The pellet was washed three times with ethanol, dried, and dissolved in 20 μl of binding buffer. Purified p53DBD (4 μg) was added, and the complex was allowed to form for 30 min on ice. Samples were loaded on a mobility shift gel as described above, and the bound and unbound fractions were eluted from the gel, precipitated with ethanol, cleaved with 1 M piperidine at 90 °C, and analyzed on a sequencing gel. Control DNA was also treated with dimethyl sulfate under identical conditions and was analyzed on the gel.

Ethylation Interference Assay—The labeled oligonucleotides were placed in 50 mM sodium cacodylate, pH 7.0, 1 mM EDTA (100 μl) and were mixed with 1 μg of salmon sperm DNA. Each sample was treated with 100 μl of saturated solution of *N*-ethyl-*N*-nitroso urea in ethanol at 50 °C for 1 h. The DNA was precipitated with 20 μl of 3 M sodium acetate and 500 μl of ethanol. The pellet was washed with ethanol, dried, and redissolved in 20 μl of binding buffer. Purified p53DBD (4 μg) was added, and the complex was allowed to form for 30 min. Samples were mixed with 4 μl of 15% Ficoll and loaded on the retardation gel. The bound and unbound fractions were eluted from the gels as described previously, ethanol-precipitated, and dissolved in 30 μl of sodium phosphate, pH 7.0, and 1 mM EDTA. Each sample was treated with 5 μl of 1 M sodium hydroxide at 90 °C for 30 min. The reaction was quenched with 5 μl of 1 M HCl, followed by 1 μl of glycogen solution (10 mg/ml) and 100 μl of ethanol. The DNA was precipitated and washed with 70% ethanol, dried, heat-denatured in formamide, and loaded on a sequencing gel.

Glutaraldehyde Cross-linking—Purified p53DBD (2 μg) was incu-

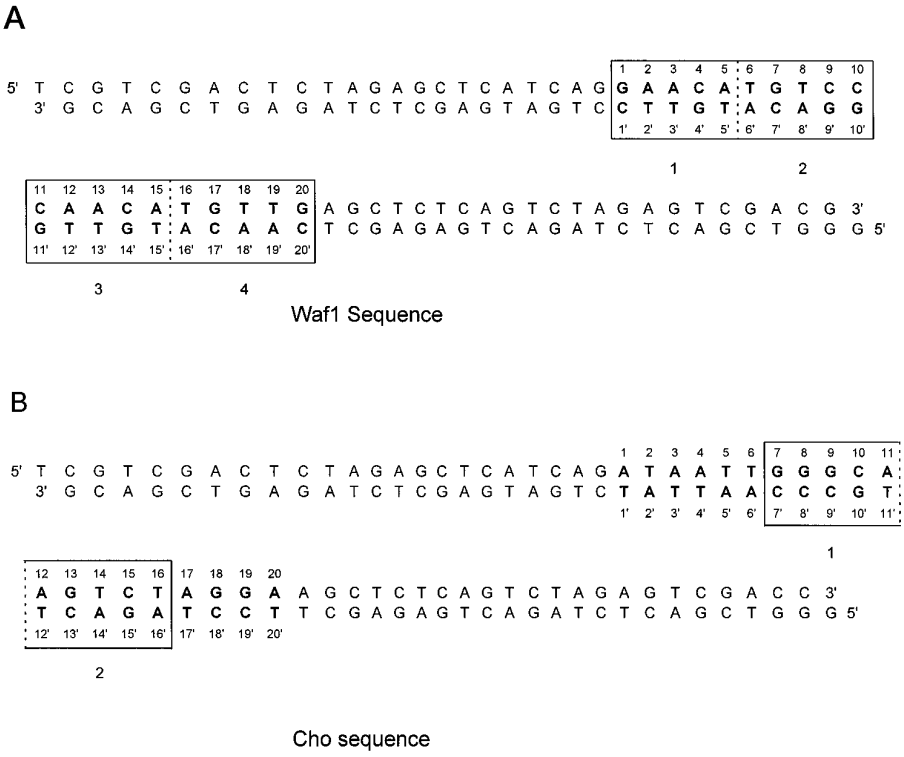

FIG. 1. *A*, 65-mer oligonucleotide containing the 20-bp *p21/waf1/cip1* response element (*boldface type* and *boxed*). *B*, 67-mer oligonucleotide containing the 20-bp Cho (18) sequence. Half-sites are separated by *solid lines*, and quarter-sites are separated by *dashed lines*.

bated in the presence of labeled oligonucleotides containing the *p21/waf1/cip1* and Cho sequences (Fig. 1, *A* and *B*) for 40 min on ice in 20 μl of DNA binding buffer. Increasing concentrations of freshly diluted glutaraldehyde were added for 15 min on ice. Partially cross-linked samples were dissociated by boiling in SDS and were loaded on an 8% SDS-polyacrylamide gel. The gel was run at 10 V/cm for 2 h and silver-stained to locate the cross-linked protein-DNA complexes. The same gel was dried and autoradiographed, and the DNA bands corresponding to the cross-linked species were located by superimposing the autoradiogram on the gel. p53DBD, used as a control in the experiment, was also treated under identical conditions. The protein molecular weight marker was heat-denatured in SDS and loaded as a control.

Electrophoretic Mobility Shift Assay—Labeled oligonucleotides of known concentration were mixed with poly(dI-dC) (200 ng) and incubated with varying amounts of p53DBD in DNA binding buffer at 4 °C for 40 min. The samples were electrophoresed on a 7% nondenaturing polyacrylamide gel in 0.25 × TBE at 4 °C. Identical unbound oligonucleotides were run in parallel. The bands were quantitated using a PhosphorImager (Bio-Rad), and the DNA binding affinities of the samples were determined as described by Carey *et al.* (22). The same gels were later used to determine the stoichiometry of p53DBD binding with the *p21/waf1/cip1* and Cho sequences (19).

DNase I Footprinting—*p21/waf1/cip1* and Cho duplexes singly end-labeled at the 5′-end of the bottom strand (3×10^5 cpm, ~200 ng) were incubated with 12 μg of p53DBD in DNA binding buffer. The complex was allowed to incubate for 40 min at 4 °C. An aliquot of the sample was checked on a nondenaturing polyacrylamide gel to ensure complete saturation of the DNA binding sites with p53DBD. The samples were mixed with 5 mM $MgCl_2$ and 10 mM $CaCl_2$ (50 μl) and digested with DNase I (13.2 ng) for 30 s on ice. The digestion was stopped by adding 90 μl of a stop solution (0.2 M NaCl, 30 mM EDTA, 1% SDS, and 100 μg/ml tRNA). The samples were extracted with phenol:chloroform, precipitated with ethanol, washed with 70% ethanol, dried, electrophoresed on a 12% denaturing polyacrylamide gel, and autoradiographed.

G and G + A Cleavage, Gel Electrophoresis, and Densitometric Scanning—The control G and G + A cleavage reactions were carried out using the now standard protocol reported by Maxam and Gilbert (23). Sequencing gels used to analyze the DNA samples contained 12% acrylamide (19:1 ratio of acrylamide:bisacrylamide) and 8 M urea. The gels were run for 2–3 h at 1500 V in 1 × TBE buffer, dried, and autoradiographed. Autoradiograms were scanned and analyzed using NIH Image, a public domain gel analysis program, and were quantitated using standard methods (24).

Model Building—To generate stereochemically acceptable DNA structures, the program DNAminiCarlo was used (25, 26). The generalized coordinates of bases and deoxyriboses served as independent parameters, and the sugar-phosphate chain was closed so that the bond lengths and angles had standard values. Various straight and bent DNA conformations were considered, among them (i) a 20-mer from the p53-DNA complex (18); (ii) regular uniform B-DNA with identical dimeric step parameters averaged over ~40 B-DNA crystal structures (26); (iii) nonuniform B-like DNA with the *p21/waf1/cip1* sequence, the dimeric steps having sequence-dependent conformations corresponding to the averages taken from ~40 protein-DNA complexes (26); and (iv and v) bent DNA modeled similarly as in conformation iii but with roll angles in the CA:TG dimers occurring at the junctions between the adjacent pentamers. Specifically, the CA roll angle was 6° in the structure modeled in conformation iii and either 15° (iv) or 20° (v). In the cocrystal structure (18), this roll angle was 4°, and it is 0° in uniform B-DNA. To account for the rigidity of the sugar-phosphate backbone and the correlation between roll and twist, the CA twist in the latter two structures was reduced from 36° (conformation iii) to 31 and 28° in conformations iv and v, respectively (26). The protein domains were positioned with respect to the *p21/waf1/cip1* response element DNA in the following way. The p53 domain, together with the pentamer GGGCA:TGCCC from the cocrystal structure to which it is bound specifically in that study (18), was superimposed on a pentamer quarter-site from the *p21/waf1/cip1* response element. For this purpose, the $C^{1'}$ atoms were used; the r.m.s. deviation was never more than 0.6–0.7 Å. Following this procedure, the p53-DNA complexes were analyzed to evaluate the closest peptide-peptide contacts reported here. It was found that, in all cases when p53 domains were bound to unbent DNAs (*i.e.* with unadjusted CA roll angles as modeled in conformations i–iii), unacceptable steric clashes occurred. By contrast, all clashes vanished in the bent DNA models (iv and v).

RESULTS

Hydroxyl Radical Footprinting of p53DBD with p21/waf1/cip1 and Cho Sequences—Hydroxyl radical cleavage (27) was used to footprint p53DBD complexed with the *p21/waf1/cip1* and Cho sequences (Fig. 1, *A* and *B*). Fig. 2, *A* and *B*, shows hydroxyl radical footprinting data for the p53DBD-*p21/waf1/cip1* and p53DBD-Cho complexes, respectively. Densitometric plots of the various lanes are shown in Fig. 2, *E* and *F*. The top strand of the naked *p21/waf1/cip1* response element (as presented in Fig. 1*A*) shows reduced cleavage at CATG and TGTT base sequences within the 20-bp consensus binding site, with clear minima at TG sequence elements (marked as *arrows* in

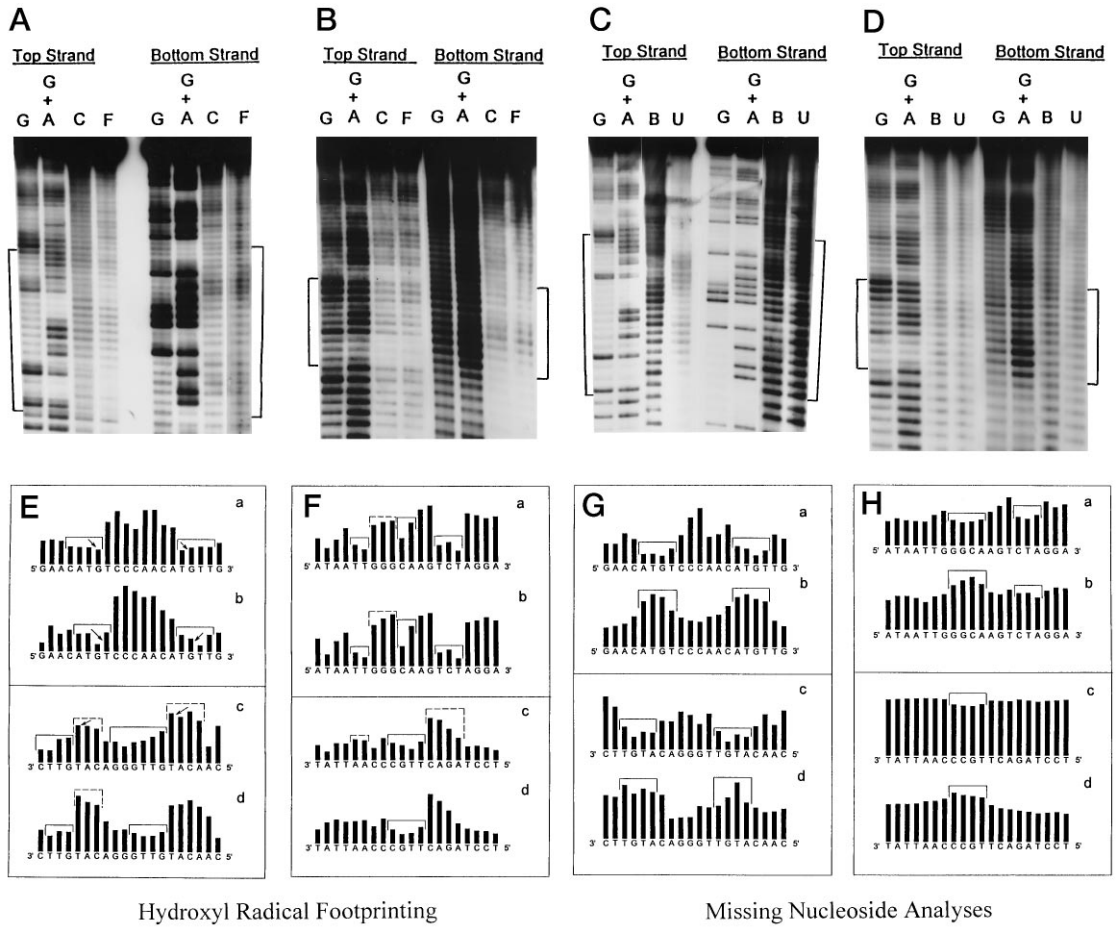

FIG. 2. **Hydroxyl radical cleavage (footprinting) (*panels A, B, E,* and *F*) and missing nucleoside analyses (*panels C, D, G,* and *H*).** *Lanes G* and *G + A* are Maxam-Gilbert guanosine and guanosine + adenosine sequencing reactions. *Vertical brackets* in *panels A–D* locate the p53 binding sites. *Panels A* and *C*, 65-mer oligonucleotide containing the p53DBD-*p21/waf1/cip1* complex (Fig. 1*A*); *panels B* and *D*, 67-mer oligonucleotide containing the p53DBD-Cho complex (Fig. 1*B*). In *panels A* and *B*, *lanes C* and *F* refer to the absence (control) and presence of p53DBD, respectively. In *panels C* and *D*, *lanes B* and *U* refer to bound and unbound fractions, respectively. *Panels E–H* are densitometric plots corresponding to the gels in *panels A–D*, respectively. *Plots a* and *b* are cleavage patterns of the top strand in the absence and presence of p53DBD, respectively. *Plots c* and *d* are similar except for the bottom strand. The *arrows* indicate maxima or minima in the cleavage patterns (see "Results"). In *panels E* and *F*, *solid brackets* indicate bases showing reduced cleavage and dashed brackets higher cleavage frequency. In *panels G* and *H*, *solid brackets* indicate bases specifically discussed under "Results."

Fig. 2*E*, *plot a*) and a higher cleavage at the central CCCAAC bases (Fig. 2*A*, *lane C*; Fig. 2*E*, *plot a*). The two TG base elements are separated by 10 bp and hence are spatially in phase along the helix. p53DBD binding shifts the cleavage frequency minimum by one base toward the 3′-end and further diminishes the cleavage frequency at ATGT and TGTT sequences, while the central CCCAAC bases show a relative increase in the cleavage frequency (Fig. 2*A*, *lane F*; Fig. 2*E*, *plot b*). The bottom strand exhibits a significantly reduced cleavage at the GTTGGG and GTTC sequences and an increased cleavage at the ACAT and CAT base sequences with maxima at TA sequence elements (marked as *arrows* in *dashed brackets*, Fig. 2*A*, *lane C*; Fig. 2*E*, *plot c*). The binding of p53DBD further enhances the cleavage frequency of CAT sequence while reducing it in the central GTTG and GTT sequences (Fig. 2*A*, *lane F*; Fig. 2*E*, *plot d*).

The unique hydroxyl radical cleavage profiles suggest that the *p21/waf1/cip1* response element has narrowed minor grooves at CATG and TGTT sequences and a relatively wider minor groove at the CCCAA sequence. p53DBD binding further narrows the minor grooves involving ATGT and TGTT bases in the two half-sites, compresses the major groove at the GTTGGG bases, and shields their sugar-phosphate backbone from the minor groove side, leading to their reduced cleavage. This may, in turn, further expose the sugar-phosphate backbone of the complementary CCCAA sequence from the minor groove side, making it more susceptible to hydroxyl radical cleavage. x-ray crystallography (28) and model building (25) on a variety of DNA sequences indicate that the minor groove width in the ACA|TGT sequence in the first half-site should be characterized by the distances between sugar moieties of G^7 and $G^{4'}$ and the phosphate distances of G^7–$T^{3'}$ and $G^{4'}$–T^8 and by the similarly positioned nucleotides in the second half-site (Fig. 5*A*, *b*). Hydroxyl radical data indicate that p53DBD binding drastically reduces the cleavage frequency in the G^7 and T^8 in the first half-site and in G^{17} and T^{18} in the second half-site (Fig. 2*E*, *a* and *b*), whereas in the bottom strand, the cleavage frequency of G^4 and $G^{14'}$ is reduced upon p53DBD binding (Fig. 2*E*, *c* and *d*). Since hydroxyl radical cleavage is a diffusion-controlled process, the data clearly point to a relatively narrow minor groove in the CATG regions in the two half-sites, which is in accord with the crystal structure data (18).

The higher cleavage at the ACAT and CAT bases in the bottom strand as compared with the ATGT and TGTT sequence at the top strand probably indicates asymmetric distortion of the double helix in this region, leading to differential exposure of the sugar-phosphate backbone of the two strands to hydroxyl radicals. The relatively A/T-rich regions of the consensus binding site, which have narrow minor grooves, are spaced at integral helical periodicity and occur on the same face of the double

helix (Fig. 5*A*). It is also of interest that GGGC sequences, previously shown to have major groove-directed bending (29–31), occur in the central region of many functionally important p53 response elements. The helically phased CA:TG sequence elements in the highly conserved region of the consensus binding site have been shown to be kinked in the CAP nucleoprotein complex (32) and may be similarly kinked in other regulatory complexes (33). Thus, it is possible that intrinsic flexibility in these sequence elements may promote the formation of a more stable p53-DNA complex by facilitating specific protein-DNA and protein-protein interactions. A recent study from this laboratory has shown that p53DBD binds the *p21/waf1/cip1* response element as a tetrapeptide with high cooperativity and that the DNA is bent by ~50–60° in solution (19). Thus, it is likely that a region of compressed major groove, located between two regions of narrow minor groove, as suggested by the present hydroxyl radical footprinting, may provide the structural basis for such a bending. We also observe that there is an inherent asymmetry in the footprinting patterns for the two half-sites, which otherwise might be expected to be identical. We believe that such an inherent asymmetry in the complex may play a crucial physiological role in terms of bending directionality, as in the case of the TATA-binding protein-TATA complex (34).

The hydroxyl radical cleavage patterns for the Cho sequence (Fig. 1*B*) and its complex with p53DBD are shown in Fig. 2*B*, and densitometry plots are shown in Fig. 2*F*. The top strand of the unbound Cho sequence shows reduced cleavage at the TCT and the CA sequence elements within the consensus half-site, while a higher cleavage frequency occurs at the GGG bases (marked with *dashed brackets*). The cleavage frequency is also markedly reduced at a TT element outside this half-site (Fig. 2*B*, *lane C*; Fig. 2*F*, *plot a*). Binding with p53DBD further diminishes the cleavage frequency of the TCT and TT sequences, while it enhances the cleavage frequency in the GGG bases (Fig. 2*B*, *lane F*; Fig. 2*F*, *plot b*). However, cleavage in the bottom strand is enhanced in the complementary AGAC and AA sequences and reduced in the TTGC bases. Binding with p53DBD further reduces the cleavage pattern in the TTGC sequence. The data clearly point to a narrow minor groove in the TCT sequence and a relatively compressed major groove in the GGGC region. These footprinting data are in general agreement with the crystallographic results (18), in which a narrowed minor groove was observed in the TCTAG sequence due to high propeller twisting. However, the cleavage pattern in the GGGCAA region demonstrates a relatively compressed and shielded major groove and indicates binding of p53DBD in this region, consistent with the crystallographic results (18).

Missing Nucleoside Experiments—Specific base contacts for both complexes were determined using missing nucleoside experiments (35). Fig. 2, *C* and *D*, show the missing nucleoside data for the p53DBD-*p21/waf1/cip1* and p53DBD-Cho complexes respectively; corresponding densitometric plots are shown in Fig. 2, *G* and *H*. The bound fraction of DNA in the top strand of p53DBD-*p21/waf1/cip1* complex (Fig. 1*A*) leads to weaker bands for bases in the two ATGT sequence elements in each half-site and intense bands for bases in the central CCCAAC sequence (Fig. 2*C*, *lane B*; Fig. 2*G*, *plot a*). The opposite pattern is observed in the unbound fraction, *i.e.* bands corresponding to bases in the central CCAA region are weak, whereas bands for bases ATGT in both of the half-sites are more intense (Fig. 2*C*, *lane U*; Fig. 2*G*, *plot b*). In the bottom strand, the protein-bound DNA shows weaker bands for bases in ATGT in both half-sites, whereas in the unbound fraction these bases show intense bands (Fig. 2*C*, *lanes B* and *U*; Fig. 2*G*, *plots c* and *d*). These data clearly show that ATGT sequence elements in both half-sites of the top and bottom strands make important contacts with the bound protein. The modification or absence of either of these base contacts greatly reduces the affinity of p53DBD with DNA. It is significant that these bases show reduced cleavage in direct hydroxyl radical footprinting (Fig. 2, *A*, *B–E*, and *F*), suggesting a narrow minor groove in these regions and further substantiating their direct involvement in the stability of the nucleoprotein complex.

Missing nucleoside data for the p53DBD-Cho complex are shown in Fig. 2*D* with corresponding densitometric plots in Fig. 2*H*. The top strand of the bound fraction shows relatively weak bands in the GGCA and CTA sequence elements (Fig. 2*D*, *lane B*; Fig. 2*H*, *plot a*). In the unbound fraction, strong bands are observed in this sequence element, indicating direct contact of these bases with the bound p53DBD (Fig. 2*D*, *lane U*; Fig. 2*H*, *plot b*). The bottom strand in the bound fraction shows weak bands in the TGCC element, while in the unbound fraction these bases exhibit much stronger bands (Fig. 2*D*, *lanes B* and *U*; Fig. 2*H*, *plots c* and *d*). Thus, the data clearly demonstrate that bases in the GGCA element in the top strand and in the TGCC element in the bottom strand make critical contacts with the bound peptide. Most of the contact sites probed by hydroxyl radical footprinting and missing nucleoside probing in the p53DBD-Cho complex are also observed in the crystal structure data (18).

Methylation Interference Assays—Methylation interference assays have been widely used to identify contacts between bound proteins and methylated guanosines in the major groove of the DNA (36). Fig. 3*A* shows the methylation interference results for the p53DBD-*p21/waf1/cip1* complex. Corresponding densitometric plots of the different lanes are shown in Fig. 3*E*. The bound DNA fraction of the top strand (Fig. 1*A*) shows reduced cleavage (greater interference) at the guanosines in the two TG sequence elements (G^7 and G^{17} in Fig. 1*A*) compared with more intense cleavage at these sites in the unbound fraction (Fig. 3*A*, *lanes B* and *U*; Fig. 3*E*, *plots a* and *b*). This suggests that these guanosines are in direct contact with p53DBD in the major groove. In the bottom strand, the bound DNA fraction shows reduced cleavage of guanosines at the two TG elements ($G^{4'}$ and $G^{14'}$) compared with much stronger bands in the unbound DNA fraction (Fig. 3*A*, *lanes B* and *U*; Fig. 3*E*, *plots c* and *d*). The residues in the central GGG region of the bottom strand show reduced cleavage in the bound DNA fraction as compared with the control DNA (*lane C*), but these guanosine signals are missing entirely from the unbound fraction.

These data clearly show that the central GGG guanosines in the bottom strand contact the p53DBD differently from those in the two TG elements. Methylation of the former does not affect p53DBD binding, whereas the guanosines in the TG doublets evidently make structurally important contacts with the protein, probably at the N-7 position, and when these sites are modified by methylation, p53DBD does not bind to DNA. It is important to note that TG guanosines are present in each pentamer quarter-site and constitute the invariant base in most of the high affinity p53 binding sites reported so far. All four guanosines in the TG base doublets (G^7, G^{17}, $G^{4'}$ and $G^{14'}$) are tandemly arrayed in the alternate major groove of the double helix, suggesting that all four subunits of p53DBD bind in the major groove.

The methylation interference data for the p53DBD-Cho complex are shown in Fig. 3*B* with corresponding densitometric plots in Fig. 3*F*. In the top strand, the p53DBD-bound fraction shows relatively weaker bands for the GGG (G^7, G^8, G^9) sequence and G^{13} compared with the unbound fraction (Fig. 3*B*, *lanes B* and *U*; Fig. 3*F*, *plots a* and *b*). In the bottom strand,

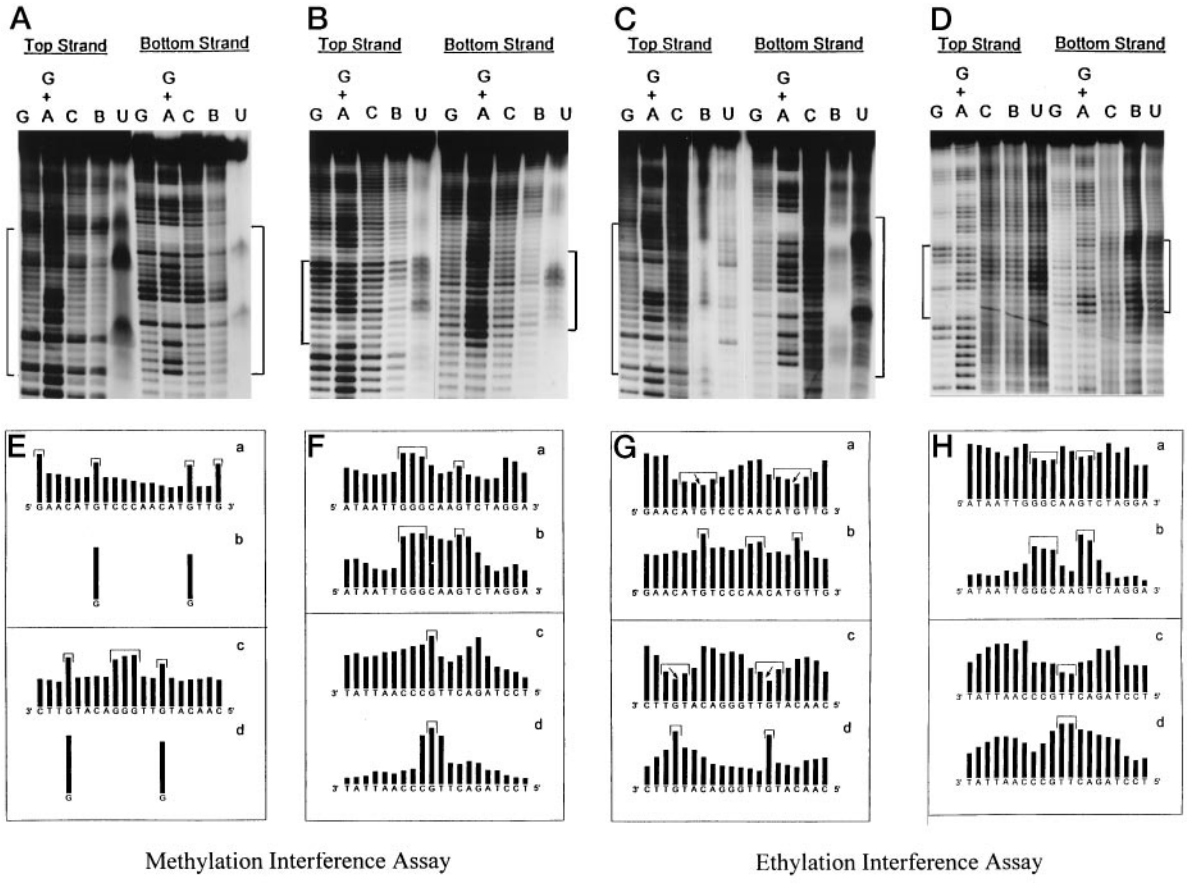

FIG. 3. **Interference assays: methylation (*panels A, B, E,* and *F*) and ethylation (*panels C, D, G,* and *H*).** Lane identification markers are the same as in Fig. 2 with the following exceptions. *Lanes C* are controls with dimethyl sulfate modification (methylation) and *N*-ethyl-*N*-nitroso urea modification (ethylation) of the DNA in the absence of p53DBD. *B* and *U* refer to bound and unbound fractions, respectively. In *panels E–H*, *solid brackets* indicate bases specifically discussed under "Results."

both the bound and unbound fractions show relatively intense bands for guanosine $G^{10'}$, with the stronger band observed in the unbound DNA fraction. The data clearly indicate that the bases G^7, G^8, G^9, and G^{13} in the top strand and $G^{10'}$ in the bottom strand make direct contact with the bound peptide, which is consistent with the cocrystal structure (18) in which Arg^{283} and Lys^{120} are in direct contact with G^7 and G^8, while Arg^{280} contacts $G^{10'}$. G^{13} (top strand) either makes direct contact with p53DBD at its N^7 position or is in very close proximity with the peptide in the complex. This observation is also consistent with the cocrystal structure in which the sugar-phosphate backbone of G^{13} and T^{14} makes direct contact with Arg^{248}. We do not observe contacts between p53DBD and bases in the GGA sequence element at the end of the top strand, *i.e.* G^{18}, G^{19} and A^{20}, as observed in the cocrystal structure.

Ethylation Interference Assays—Sugar-phosphate contacts were probed by ethylation interference (37). Results for the p53DBD-*p21/waf1/cip1* complex are shown in Fig. 3*C* with corresponding densitometric plots of the bound and unbound fractions shown in Fig. 3*G*. For the top strand (Fig. 1*A*), the bound fraction shows weaker bands for bases in the ATGT sequence elements in the two half-sites with clear minima at the two TG base doublets (Fig. 3*C*, *lane B*; Fig. 3*G*, *plot a*), whereas in the unbound fraction, these two guanosine residues show significantly more intense bands (Fig. 3*C*, *lane U*; Fig. 3*G*, *plot b*). The AA sequence elements at the center of the binding site also appear as bands of medium intensity. For the bottom strand, the bound fraction (Fig. 3*C*, *lane B*; Fig. 3*G*, *plot c*) shows weaker bands in TGT sequence elements in both half-sites, with clear minima at the G residues (marked as *arrows*). On the other hand, bases in the TG elements appear as highly intense bands in the unbound fraction (Fig. 3*C*, *lane U*; Fig. 3*G*, *plot d*). These data clearly indicate that the DNA backbone at the ATGT sequences in the two half-sites is in contact with the p53DBD in the complex, which is consistent with the hydroxyl radical and missing nucleoside data. Particularly, the sugar-phosphate backbone at G^7, G^{17}, $G^{4'}$, and $G^{14'}$ makes very critical contacts with p53DBD, and ethylation of phosphates at these residues greatly reduces the binding affinity of the p53DBD-*p21/waf1/cip1* complex.

Fig. 3*D* shows ethylation interference results for the p53DBD-Cho complex with densitometric plots in Fig. 3*H*. For the top strand (Fig. 1*B*), the bound fraction shows relatively weak bands in the GGC and GT elements of the consensus binding site, whereas in the unbound fraction these bands are much stronger (Fig. 3*D*, *lanes B* and *U*; Fig. 3*H*, *plots a* and *b*). The GT bases, in particular, show very strong signals in the unbound fraction, indicating direct contact of p53DBD with the sugar-phosphate backbone. For the bottom strand, the bound fraction shows much weaker bands in the TT region but much stronger bands in the unbound fraction, again indicating direct contact of p53DBD with the backbone. Our data are in excellent agreement with the sugar-phosphate backbone contacts observed in the cocrystal structure in which Arg_{248} makes direct backbone contacts with these bases (18).

The Binding of p53DBD to the p21/waf1/cip1 and Cho Binding Sites—Fig. 4 shows the results of several studies on the binding stoichiometry and positioning of the p53DBD peptide on the two DNA binding sites investigated. Glutaraldehyde cross-linking (38, 39) was used to determine the stoichiometry

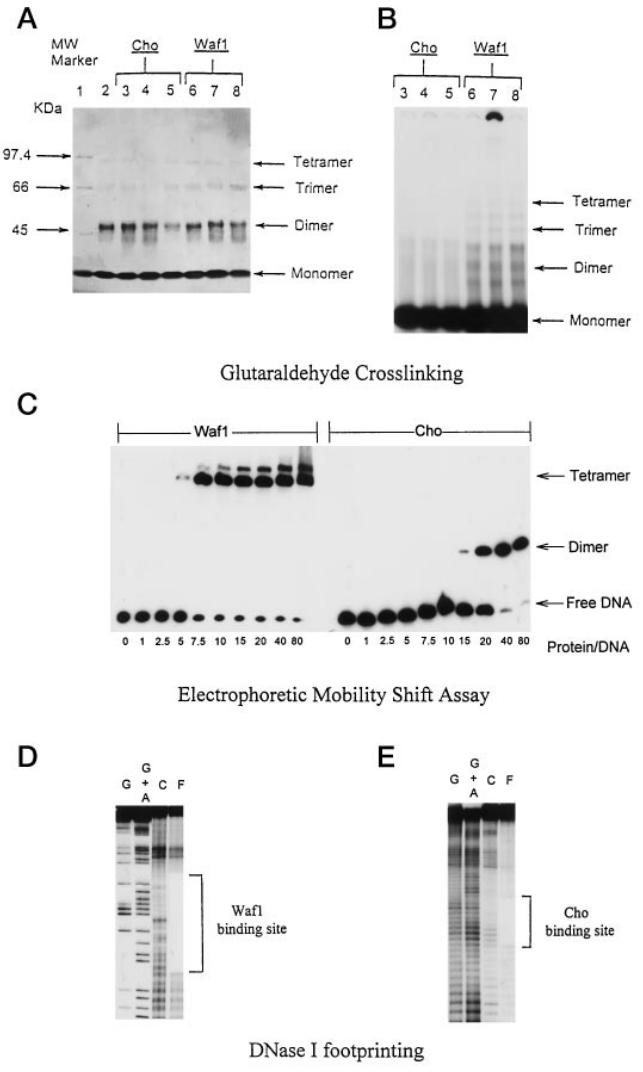

FIG. 4. **Glutaraldehyde cross-linking of p53DBD with oligonucleotides containing *p21/waf1/cip1* and Cho sequences (Fig. 1, *A* and *B*).** *A*, 8% SDS-polyacrylamide gel followed by silver staining. *Lane 1*, protein molecular weight markers. *Lane 2*, p53DBD cross-linked in the absence of DNA. *Lanes 3*, *4*, and *5*, different oligomeric states of p53DBD cross-linked to the Cho oligonucleotide in the presence of 0.01, 0.05, and 0.1% glutaraldehyde, respectively. *Lanes 6*, *7*, and *8*, different oligomeric states of p53DBD cross-linked to the *p21/waf1/cip1* oligonucleotide in the presence of 0.01, 0.05, and 0.1% glutaraldehyde, respectively. *B*, autoradiograph of the gel in *A* showing cross-linked DNA species associated with lanes 3–8 of *A*. *C*, electrophoretic mobility shift assay of the *p21/waf1/cip1* and Cho sequences. The molar ratios of p53DBD to DNA are given at the bottom of the gel. *D* and *E*, DNase I footprinting of the *p21/waf1/cip1* and Cho sequences, respectively. The *lanes* marked *G* and *G* + *A* are the Maxam-Gilbert sequencing reactions; *lanes C* and *F* are control DNA and DNA with p53DBD, respectively.

of p53DBD bound to the *p21/waf1/cip1* and Cho response elements. Fig. 4*A* shows an SDS-polyacrylamide gel electrophoresis analysis of the cross-linked species of the p53DBD-*p21/waf1/cip1* complex (Fig. 4*A*, *lanes 6*, *7*, and *8*) and the p53DBD-Cho complex (*lanes 3*, *4*, and *5*) at three glutaraldehyde concentrations. The p53DBD-*p21/waf1/cip1* complex shows four bands of 23, 46, 69, and 92 kDa, representing monomer, dimer, trimer, and tetramers, respectively. Direct autoradiography confirms that each band is associated with its corresponding DNA fragment (Fig. 4*B*, *lanes 6*, *7*, and *8*). This demonstrates clearly that the p53DBD peptide associates with the full *p21/waf1/cip1* response element as a tetrapeptide, even in the absence of the wild type p53 oligomerization domain, in agreement with gel band shift and ultracentrifugation results (19). With the p53DBD-Cho half-site, cross-linked species include trimers and tetramers in the SDS-polyacrylamide gel (Fig. 4*A*, *lanes 3–5*) but only monomers and dimers in the autoradiography (Fig. 4*B*, *lanes 3–5*). This indicates that p53DBD associates with the Cho sequence primarily as a monomer or dimer. The p53DBD peptide cross-linked in the absence of response elements can also weakly tetramerize, but the primary cross-linking products are monomers and dimers (Fig. 4*A*, *lane 2*). In Fig. 4, *A* and *B*, the DNA and protein bands move as doublets in the gel. An explanation for this commonly observed phenomenon may be that the faster band in each doublet arises from additional intrapeptide cross-linking and incomplete denaturation of the protein in SDS, leading to a more compact structure for the denatured complex and therefore slightly higher mobility (39).

A gel electrophoretic mobility shift assay was used to determine the binding affinity and stoichiometry of the p53DBD with the *p21/waf1/cip1* and Cho sequences and is shown in Fig. 4*C*. It is evident that p53DBD binds the *p21/waf1/cip1* response element only as a tetramer with high cooperativity. We assign the minor bands of slightly lower mobility than the tetramer complex to the nonspecific binding of p53DBD with the single-stranded duplex overhangs (40, 41). No intermediate bands, *e.g.* dimer or trimer, are evident. We estimate a mean equilibrium dissociation constant, K_d, of 4.2×10^{-9} M for the p53DBD-*p21/waf1/cip1* complex, which is in satisfactory agreement with the value $(8.3 \pm 1.4) \times 10^{-8}$ M obtained by analytical ultracentrifugation (19), since the ~5-fold difference most probably results from a lower dissociation rate of the complex in the gel (42). In the case of the Cho sequence, p53DBD binds as a dimer with an estimated mean equilibrium dissociation constant K_d of 7.8×10^{-7} M. This level of binding affinity is not much greater than that for many nonspecific nucleoprotein complexes. However, there is no evidence in Fig. 4, *B*, *C*, and *E*, for the association of a third p53DBD monomer as was observed in the cocrystal (18).

Fig. 4, *D* and *E*, show DNase I footprint results for p53DBD binding to the *p21/waf1/cip1* and Cho sequences, respectively, at saturating protein concentrations. With the *p21/waf1/cip1*, the footprint is extremely tight, spanning all 20 bp of the response element and exhibiting absolutely no evidence of nonspecific binding (Fig. 4*D*, *lane F*). This footprint is similar to that observed for the wild type p53 protein complexed with ribosomal gene cluster response element (43). These data suggest that p53DBD is tightly associated with the response element, thereby excluding completely the possibility of digestion of the DNA by the enzyme. A tight footprint is also seen with the Cho sequence under identical conditions, which covers completely the 10-bp half-site (Fig. 4*E*, *lane F*). As in the *p21/waf1/cip1* complex, the data show no evidence for peptide binding at any location other than at the specific binding sites.

DISCUSSION

A Comparison of the Footprinting Data for p53DBD Complexed with the p21/waf1/cip1 and Cho Sequences—We have summarized the above results on the p53DBD-*p21/waf1/cip1* and p53DBD-Cho complexes in Figs. 5, *panels A* and *B*, respectively. For the p53DBD-*p21/waf1/cip1* complex, certain structurally related characteristics become immediately apparent. (i) Most of the contact signals occur in the major groove of the DNA in a staggered array along the two helical turns of the response element in which each of the four bound p53DBD peptides occupies a single pentanucleotide quarter-site and faces outward, away from the DNA, in the same direction. The data indicate that each p53DBD binds to the major groove in agreement with the cocrystal structural study (18). (ii) Four

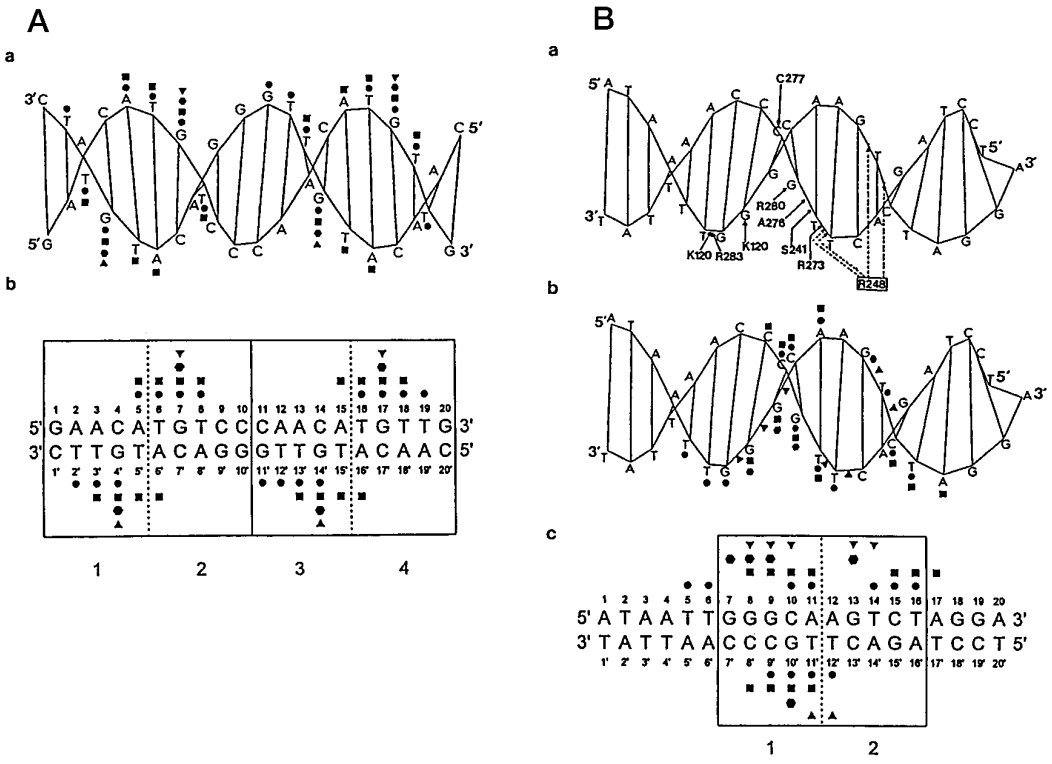

FIG. 5. *A*, helical representation (*a*) and sequence (*b*) of the 20-bp *p21/waf1/cip1* response element showing contact sites identified by the chemical footprinting techniques. The helix was generated using wedge angle parameters as described by Bolshoy *et al.* (50) and the CURVATUR program (63), which simulates the double helix by joining $C^{1'}$ atoms in paired nucleotides. For simplicity of presentation and comparison with the sequence (*b*), the helical DNA is represented as unkinked. Indicated contacts are as determined by protection from hydroxyl radical cleavage (●); missing nucleoside experiments (■); ethylation interference signals in the sugar-phosphate backbone (▲); and methylation interference assays (●). *B*, helical representations (*a* and *b*) and sequence (*c*) of the 20-bp Cho sequence. Generation of the helical models and symbols indicating peptide-DNA contacts are as in *A*. The helical models show contact sites observed in the cocrystal structure (18) (*a*), and contact sites observed in the present chemical probe studies (*b*).

guanosine bases, G^7 and G^{17} in the top strand and $G^{4'}$ and $G^{14'}$ in the bottom strand, which are part of an invariant sequence motif in each pentamer quarter-site, are identified as contacts in all of the four footprinting techniques used. These bases are in phase along the helix with a separation of 10 bp and are located in the major groove of the DNA. (iii) Most of the observed contact points are clustered in the major groove with relatively few contacts in the minor groove also in agreement with the specifically bound p53DBD in the crystal structure (18). (iv) The GTTG sequence of the bottom strand shows higher protection from hydroxyl radical cleavage than does the complementary CAAC sequence on the opposite strand, suggesting that it is shielded by bound peptide from the minor groove side, whereas the complementary CAAC sequence is exposed.

For the p53DBD-*p21/waf1/cip1* nucleoprotein complex, the present results are most consistent with a model in which all four p53DBD peptides make their most important contacts between the major groove of the response element DNA with their loop sheet helix motif. The p53DBD peptides are bound to the major groove of each pentameric quarter-site in an alternating array so that, apart from DNA bending, the full complex possesses a quasi-C_2 symmetry. The data also require that the conserved guanosines of each pentamer half-site play a crucial role in the binding. This model is not generally appropriate for the p53DBD-Cho complex, however. In this complex, the hydroxyl radical and the missing nucleoside contacts are symmetrical along the DNA, and the methylation and ethylation interference signals and some of the missing nucleoside contacts show a marked asymmetry. The footprinting contacts are arranged very differently from those in the *p21/waf1/cip1* complex and suggest that there are two binding sites in the Cho sequence in opposite orientations along the DNA. One is to the GGGCA quarter-site element in the upper strand (Fig. 1*B*; Fig. 5*B*, *c*), and the second is to the TGCCC element in the lower strand. Contacts in the first of these are consistent with those observed in the cocrystal structure (Fig. 5*B*, *a*) (18), and since this is the only specific binding site observed crystallographically, it is likely that it is a site of higher binding affinity. A direct repeat of TGCCT, having close homology with the TGCCC element in the Cho sequence, has previously been shown to be a functionally important p53 binding site (44, 45).

The relatively lower quality of the footprinting data for the p53DBD-Cho complex compared with the *p21/waf1/cip1* complex suggest that, in solution, a dynamic equilibrium may exist between complexes involving these two sites. In the *p21/waf1/cip1* response element, all the four invariant guanosines occur in the TG sequence elements. By contrast, in the Cho sequence, only one guanosine occurs in the TG element, whereas the other occurs in an AG element. Since we observe intense contact signals for the guanosines in the *p21/waf1/cip1* TG elements but not in the Cho half-site AG, this suggests that AG elements are very poor contact sites for p53 binding. Again, these results are consistent with earlier observations (18, 46).

Stereochemical Model for the p53-DNA Complex—To rationalize our footprinting and cross-linking data presented above, we have developed a computer-assisted structural model for the p53DBD-*p21/waf1/cip1* complex. In this model, each of the four bound p53DBD peptides is attached to a single pentameric quarter-site as suggested by the present footprinting results. The p53DBD coordinates are taken from the cocrystal structure; in that study, no changes in the p53DBD structure were observed upon DNA binding (18). Docking of the peptides to the DNA is determined by the specific contacts found here (Fig.

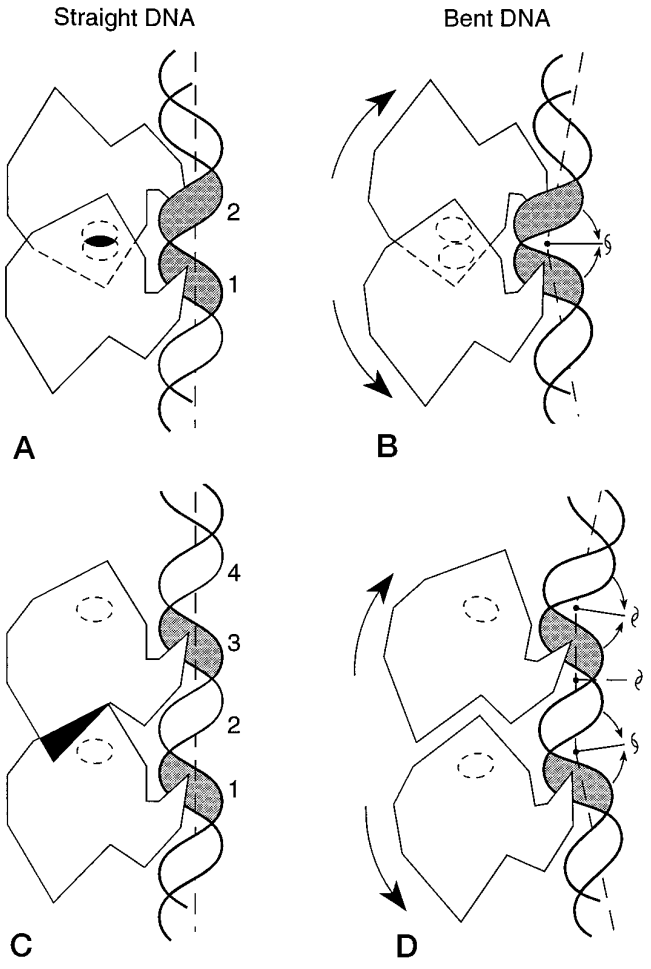

FIG. 6. **Diagrams showing how molecular modeling determines steric clashes between the four p53DBD peptides bound to the *p21/waf1/cip1* response element as directed by the chemical probe results and how these clashes are relieved by bending the DNA by a roll at the CA:TG sequence elements.** Nomenclature for p53DBD structural elements is from Cho *et al.* (18). The zinc-binding H1 helices are shown as *ellipses*. The H2 recognition helices are shown as sharply pointed regions buried in the major grooves. The four pentamer response element quarter-sites are *numbered 1–4*. Pentamers 1 and 3 and pentamers 2 and 4 are in a parallel orientation, while pentamers 1 and 2 and pentamers 3 and 4 are antiparallel. *A*, in unbent DNA, binding of two p53DBD peptides to pentamers 1 and 2 (antiparallel orientation) is accompanied by steric hindrance between the H1 helices (*overlapped ellipses*; see legend to Fig. 7*A* for details). *B*, this clash is relieved by bending the DNA toward the major groove along the dyad axis by a positive roll at the TG:CA sequence elements as discussed under "Discussion" (see legend to Fig. 7*B* for details). *C*, in unbent DNA, binding of two p53DBD peptides to pentamers 1 and 3 (parallel orientation) is accompanied by steric hindrance. The *darkened overlap area* represents steric clash between residues 99, 167, 170, and 210 from one peptide and residues 224, 140, 199, and 201 from the other; a steric clash is presumed if the distance between two heavy atoms in a residue pair is less than 2.4 Å. *D*, this clash is relieved by bending the DNA toward the major grooves along the dyad axes at two points separated by 10 bp. This bending is the same as in *B* and is affected by a positive roll at the TG:CA sequence elements as discussed under "Discussion."

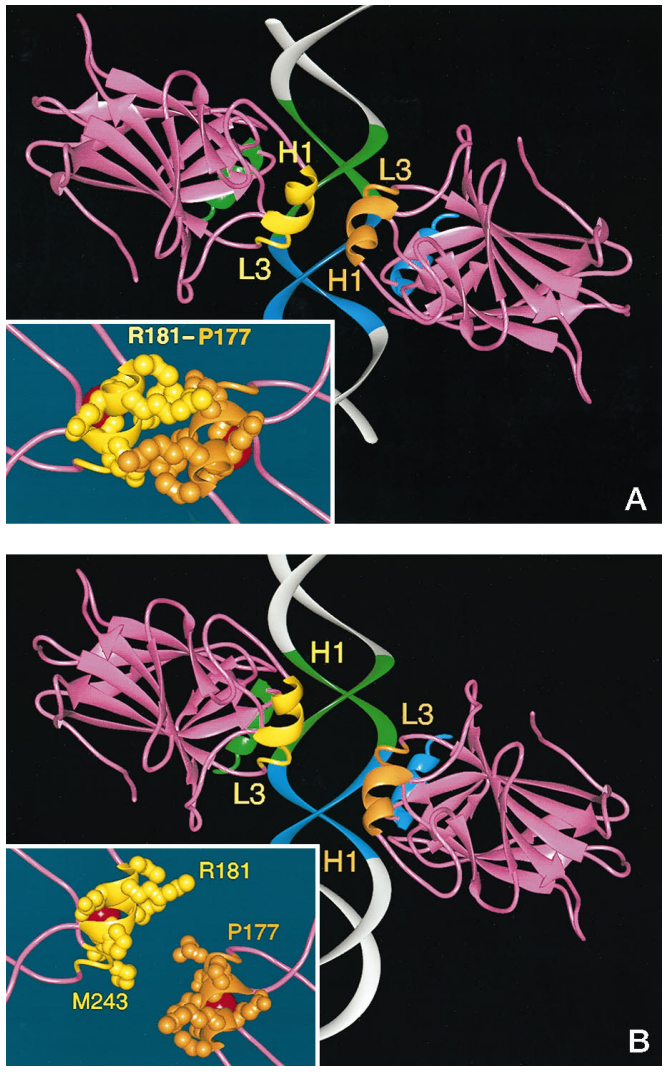

FIG. 7. **Interactions between the H1 helices and L3 loops in the p53-DNA complexes for unbent DNA (18) (*A*) and bent DNA (*B*).** *A*, the H2 helix from the left domain (*green*) interacts specifically with the pentamer GGGCA (also shown in *green*) (18). The right domain is located symmetrically, so that its H2 helix (*blue*) interacts with the pentamer AGACT shown in *blue* (for details, see "Materials and Methods"). *Inset*, the H1 helices interdigitate, producing unacceptable steric clashes (the heavy atoms in the protein are shown as spheres of 50% van der Waals radii). The zinc atoms are shown as *large red spheres*. The clashes specifically involve Arg^{181} and Pro^{177}. Similar clashes occur using other unbent DNA models including canonical B-form DNA (see "Materials and Methods"). *B*, bending the DNA toward the major groove at the junction between the *green* and *blue* pentamers relieves the H1-H1 clash (the bend is directed *away* from the viewer). The important spatial complementarity between the two H1-L3 moieties is shown in the *inset*; in this view, the protruding residues are Arg^{181} (in the H1 helix) and Met^{243} (in the L3 loop).

5*A*). The model requires that, to avoid severe interpeptide steric clashes, the four p53DBD peptides must induce bending of the response element DNA by ~50° (Fig. 8), a result in close agreement with recent cyclization studies (19) and with circular permutation gel electrophoresis assays (20). Specifically, we find two sets of steric clashes in the complex between four p53 domains and "straight" DNA. The first of these occurs between the zinc-binding H1 helices (18) of peptides bound to two adjacent pentamers (Figs. 6*A* and 7*A*); these two p53 domains are bound to opposite sides of the duplex in opposite orientations and "embrace" the DNA. The second clash occurs between the two peptides in similar orientation and bound to the same side of the helix; they are separated by a single helical turn (Fig. 6*C*). It is important to note that these clashes were observed in all complexes involving unbent DNA that were analyzed (see "Materials and Methods").

The above steric clashes are relieved if the *p21/waf1/cip1* DNA is bent by positive rolling through 15° toward the major grooves in the CA:TG dimers indicated by chemical points: GAAC·A|T·GTCCCAAC·A|T·GTTG. Such axial bending does not interfere with the specific interaction of the p53DBD peptides with their cognate pentamers. The two adjacent rolls in the

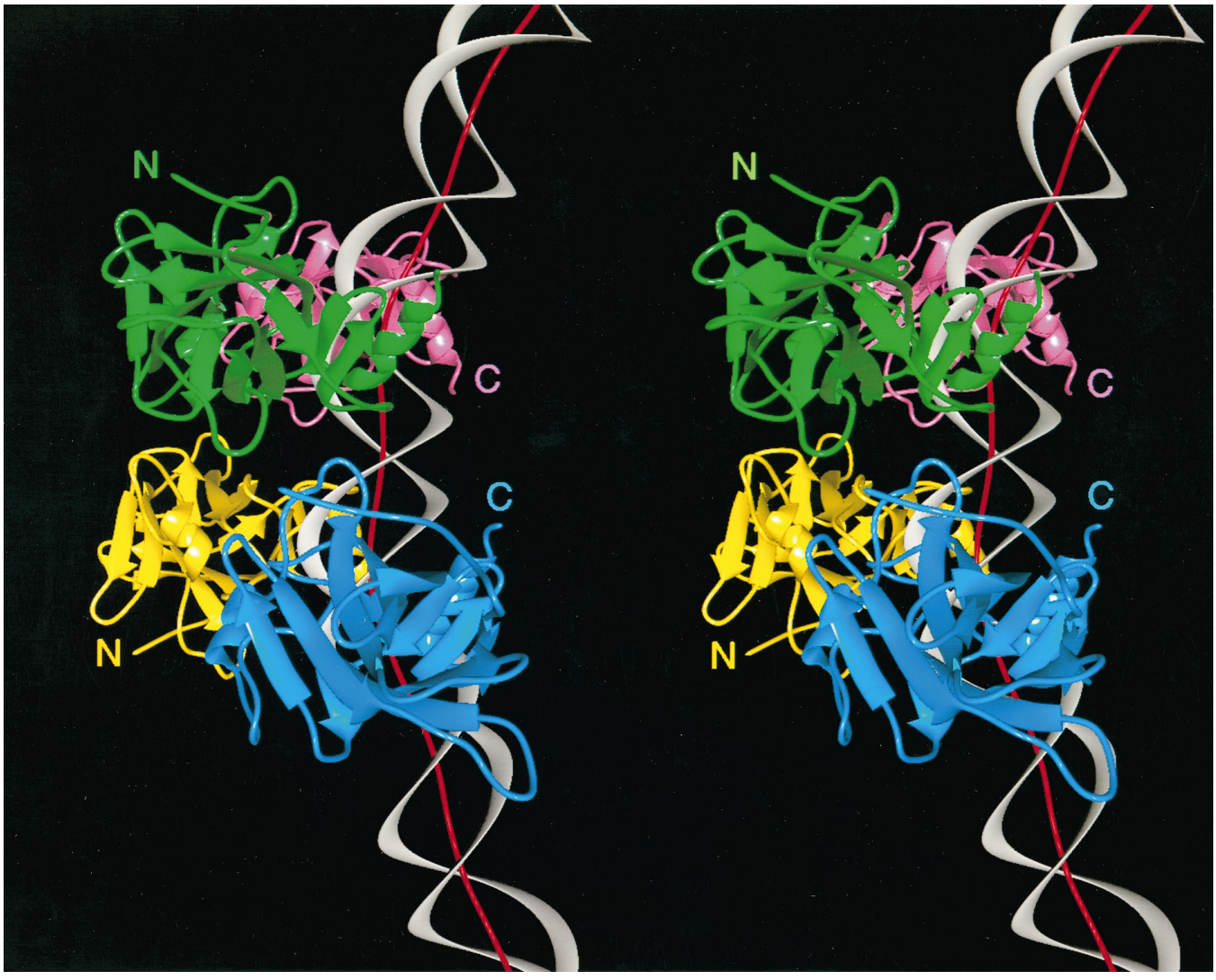

FIG. 8. **Stereo view of the putative complex between four p53DBD peptides and the *p21/waf1/cip1* response element.** The DNA axis is shown in *red* and passes through the *centers* of the base pairs (the centers of the C^6-C^8 vectors). In this model, the DNA is bent by ~50°, which relieves the steric hindrances among the bound peptides. This bending angle is consistent both with circular permutation results (20) and with recent cyclization measurements (19). The positioning of the p53DBD peptides and the DNA bending is the same as that shown in Fig. 7*B*. Note the spatial complementarity among the projecting loop in the *blue* domain and the depression in the *green* one. In this model, the N-terminal ends of the p53DBD, which attach to the transactivational domain of intact p53, are exposed on the *outside* of the DNA bend and are hence fully accessible. The C-terminal ends, which attach through a flexible region to the oligomerization and C-terminal "tail" domains, are located at the *inside* of the bend, thus facilitating tetramerization in the wild type protein and bringing the C-terminal basic regions into closer proximity with the DNA. Figs. 7 and 8 were generated using the MidasPlus program (64).

CA:TG dimers induce a bend toward the major groove as indicated in Fig. 6, *B* and *D*. It is important to note that the *same* DNA bends relieve both types of clashes: antiparallel, as in Figs. 6*A* and 7*A*, and parallel, as in Fig. 6*C*. The putative rolls in the CA:TG steps are consistent with the well known flexibility of these dinucleotides (33), demonstrated in numerous x-ray structures of pure B-DNA and protein-DNA complexes (26, 32, 47), as well as by gel electrophoresis (48). According to energy calculations, these dinucleotides can also bend anisotropically toward the major groove (25).

This direction of DNA bending is entirely consistent with the consensus p53-binding sequence. All four possible tetramers allowed by the consensus, *i.e.* CA|TG, CT|TG, CA|AG, and CT|AG, contain dinucleotide elements that can flex toward the major groove. In addition to CA:TG, the CT:AG element also prefers bending toward the major groove (26, 49, 50). AA:TT or AT:AT dinucleotides are the central elements in three of the tetranucleotides. Both dinucleotides prefer a negative or zero roll angle (26); thus, the minor groove is expected to be relatively narrow, which is desirable for interactions with the highly conserved Arg^{248} (18). The CT|AG tetranucleotide contains the TA:TA element, which can assume roll angles between −6.4° in free DNA (51) to +12° in the *trp* repressor complex (52) and appears, in addition, to possess unusual torsional flexibility (31, 32). However, the CT|AG element is reported to be extremely rare in functional genomic p53 response elements (15).

In the detailed model presented in Fig. 8, the roll angles for CA:TG are taken as 15°. This leads to an overall bend of ~50°, which is consistent both with the present experimental results and with the previous cyclization studies (19). CA:TG roll angles between 15 and 20° are sufficient to relieve all peptide-peptide clashes; 15° seems preferable, however, since this leads to a structure in which the p53DBD peptides are in close proximity to one another (Figs. 7*b* and 8) and hence can interact to produce the observed binding cooperativity (19).

According to this model, shown in Fig. 8, the C-terminal residues of p53 are located on the inside of the DNA curve. The

C-terminal domains are involved in oligomerization, protein-protein interactions, and the modulation of DNA binding (53). This arrangement may be advantageous for the stabilization of the entire superstructure in the binding of the wild type protein. On the other hand, the N-terminal region, which contains the transactivational domain, is located on the outside of the loop, where it may be more accessible to other proteins. The model presented in Fig. 8 suggests that the intrinsic bendability of p53 response elements favors the same direction of DNA bending as in the p53 nucleoprotein complex. Thus, p53 response elements may be wrapped in chromatin in such a way as to facilitate the approach and binding of the protein. In other words, p53 may prefer to bind response element DNA from the side that is normally exposed in chromatin structures. This is consistent with a transcriptional role for p53 that may be mediated by the architectural organization of chromatin (54, 55) and the looping of DNA (56).

Conclusions—The *p21/waf1/cip1* site is one of the most important functional sites for p53 binding presently known (57). The full site consists of a consensus (16) and a nonconsensus half-site, making it generally representative of a broad class of p53 response elements (15). The data presented here provide a more complete picture than previously available for the overall spatial arrangement of the peptides on the *p21/waf1/cip1* response element DNA along with critical p53DBD-DNA contacts and important information on the conformation of the binding site DNA. The footprinting and contact data show that a p53DBD is bound in the major groove on each of the four pentameric quarter-sites of the *p21/waf1/cip1* response element with the peptides oriented in the same direction. Molecular modeling shows that relief of steric clashes in the bound peptides requires the DNA to bend at flexible TG:CA sequence elements, resulting in an overall bend of ~50° over the full response element *away from the peptide complex*. Such a bending motif differs from previously observed motifs in that major groove-binding proteins usually wrap the DNA (32, 47), whereas minor groove binders bend the DNA in the direction observed here (58).

The present model is realistic in terms of p53 function, however, since it suggests that the C-terminal domains of the full p53 protein lie on the concave side of the bend and the N-terminal transactivation domain on the convex side (Fig. 8); this would be a convenient arrangement both in terms of chromatin structure and of possible allosteric regulation in the intact protein (59). In addition, wild type p53 interacts with a variety of cellular and viral oncoproteins through its acidic transactivation domain (60). The proposed arrangement of this domain coupled with inherent flexibility in the response element may facilitate the formation of such multiprotein supercomplexes. This view of the p53DBD-*p21/waf1/cip1* complex also underscores the symbiosis between the absolute structural and the chemical probes/molecular modeling approaches. Although no high resolution cocrystal structure is yet available for the p53DBD-*p21/waf1/cip1* complex, the results from the existing structural study (18) complement the chemical data presented here, and the two permit the development of a reasonable model for the full tetrapeptide complex.

It is known that TG:CA sequence elements are ubiquitous in genomic regulatory sites and particularly so in those in which DNA bending may occur in the regulatory nucleoprotein complexes (33). Various studies have shown that these elements are flexible, with potential for abrupt kinking (25, 48, 61, 62), and such kinking has been observed structurally in a limited number of nucleoprotein complexes (32, 47). Hence, it is quite likely that helically phased TG:CA or other flexible sequence elements play a critical role in the ability of p53 response elements to bend and accommodate the protein in the p53 complex, thus enhancing the stability of the complex through more precise, and perhaps more extensive, protein-DNA contacts. Most functional p53 binding sites contain helically phased TG:CA sequence elements in approximately the same relative positions (16). This requirement may also provide a structural explanation for the fact that p53 response elements that contain spacers between the palindromic half-sites have generally been observed to be highly unstable and nonfunctional (15).

The present results suggest that sequence-dependent structural and dynamical properties of the response element DNA may modulate both the stability and structure of p53 nucleoprotein complexes. This is consistent with earlier studies that demonstrated substantial DNA bending in several p53DBD-DNA complexes (19) and suggests a possible role for the variation observed in the sequences of known naturally occurring functional p53 response elements (15). The present findings support the concept that both specificity and stability of p53-DNA nucleoprotein complexes are controlled by a complex interplay of specific sequence contacts as well as inherent structural features of the DNA. In addition to deformation of the DNA and the sequence-directed requirement of the two narrow minor grooves and a compressed major groove as found in this study, these effects must include a (possibly variable) set of specific protein-DNA and intra-p53 protein-protein contacts and may also include specific or nonspecific inter-p53DBD interactions.

Acknowledgments—We thank Professor Jeffrey Hayes for a careful reading of the manuscript and for many helpful suggestions. We also thank Professor Ilga Winicov and Drs. Robert Jernigan and Stewart Durell for useful suggestions.

REFERENCES

1. Lane, D. P. (1992) *Nature* **358,** 15–16
2. Vogelstein, B., and Kinzler, K. W. (1992) *Cell* **70,** 523–526
3. Levine, A. J. (1993) *Annu. Rev. Biochem.* **62,** 623–651
4. Selivanova, G., and Wiman, K. G. (1995) *Adv. Cancer Res.* **66,** 143–180
5. Barak, Y., Juven, T., Haffner, R., and Oren, M. (1993) *EMBO J.* **12,** 461–468
6. El-Deiry, W. S., Tokino, T., Velculescu, V. E., Levy, D. B., Parsons, R., Trent, J. M., Lin, D., Mercer, W. E., Kinzler, K. W., and Vogelstein, B. (1993) *Cell* **75,** 817–825
7. Hartwell, L. H., and Kastan, M. B. (1994) *Science* **266,** 1821–1828
8. Marx, J. (1994) *Science* **266,** 1321–1322
9. Finlay, C. A., Hinds, P. W., and Levine, A. J. (1989) *Cell* **57,** 1083–1093
10. Lin, D., Shields, M. T., Ullrich, S., Appella, E., and Mercer, W. E. (1992) *Proc. Natl. Acad. Sci. U. S. A.* **89,** 9210–9214
11. Lowe, S. W., Schmitt, E. M., Smith, S. W., Osborne, B. A., and Jacks, T. (1993) *Nature* **362,** 847–849
12. Harris, C. C. (1993) *Science* **262,** 1980–1981
13. Bargonetti, J., Manfredi, J. J., Chen, X., Marshak, D. R., and Prives, C. (1993) *Genes & Dev.* **7,** 2565–2574
14. Pavletich, N. P., Chambers, K. A., and Pabo, C. O. (1993) *Genes & Dev.* **7,** 2556–2564
15. Tokino, T., Thiagalingam, S., El-Deiry, W. S., Waldman, T., Kinzler, K. W., and Vogelstein, B. (1994) *Hum. Mol. Genet.* **3,** 1537–1542
16. El-Deiry, W. S., Kern, S. E., Pietenpol, J. A., Kinzler, K. W., and Vogelstein, B. (1992) *Nat. Genet.* **1,** 45–49
17. Hollstein, M., Sidransky, D., Vogelstein, B., and Harris, C. C. (1991) *Science* **253,** 49–53
18. Cho, Y. J., Gorina, S., Jeffrey, P. D., and Pavletich, N. P. (1994) *Science* **265,** 346–355
19. Balagurumoorthy, P., Sakamoto, H., Lewis, M. S., Zambrano, N., Clore, G. M., Gronenborn, A. M., Appella, E., and Harrington, R. E. (1995) *Proc. Natl. Acad. Sci. U. S. A.* **92,** 8591–8595
20. Nagaich, A. K., Appella, E., and Harrington, R. E. (1997) *J. Biol. Chem.* **272,** 14842–14849
21. Sambrook, J., Fritsch, E. F., and Maniatis, T. (1989) *Molecular Cloning: A Laboratory Manual*, 2nd Ed., pp. 13.78–13.95, Cold Spring Harbor Laboratory, Cold Spring Harbor, NY
22. Carey, J. (1991) *Methods Enzymol.* **208,** 103–117
23. Maxam, A. M., and Gilbert, W. (1980) in *Methods Enzymol.* **65,** 499–560
24. Dixon, W. J., Hayes, J. J., Levin, J. R., Weidner, M. F., Dombroski, B. A., and Tullius, T. D. (1991) *Methods Enzymol.* **208,** 380–413
25. Zhurkin, V. B., Ulyanov, N. B., Gorin, A. A., and Jernigan, R. L. (1991) *Proc. Natl. Acad. Sci. U. S. A.* **88,** 7046–7050
26. Gorin, A. A., Zhurkin, V. B., and Olson, W. K. (1995) *J. Mol. Biol.* **247,** 34–48
27. Tullius, T. D., Dombroski, B. A., Churchill, M. E. A., and Kam, L. (1987) *Methods Enzymol.* **155,** 537–558
28. Fratini, A. V., Kopka, M. L., Drew, H. R., and Dickerson, R. E. (1982) *J. Biol.*

Chem. **257,** 14686–14707
29. Goodsell, D. S., Kopka, M. L., Cascio, D., and Dickerson, R. E. (1993) *Proc. Natl. Acad. Sci. U. S. A.* **90,** 2930–2934
30. Brukner, I., Susic, S., Dlakic, M., Sauic, A., and Pongor, S. (1994) *J. Mol. Biol.* **236,** 26–32
31. Dlakic, M., and Harrington, R. E. (1995) *J. Biol. Chem.* **270,** 29945–29952
32. Schultz, S. C., Shields, G. C., and Steitz, T. A. (1991) *Science* **253,** 1001–1007
33. Harrington, R. E., and Winicov, I. (1994) in *Prog. Nucleic Acids Res. Mol. Biol.* **47,** 195–270
34. Kim, J. L., and Burley, S. K. (1994) *Nat. Struct. Biol.* **1,** 638–653
35. Hayes, J. J., and Tullius, T. H. D. (1989) *Biochemistry* **28,** 9521–9527
36. Wissman, A., and Hillen, W. (1991) *Methods Enzymol.* **208,** 365–378
37. Siebenlist, U., and Gilbert, W. (1980) *Proc. Natl. Acad. Sci. U. S. A.* **77,** 122–126
38. Tao, X., Zeng, H. Y., and Murphy, J. (1995) *Proc. Natl. Acad. Sci. U. S. A.* **92,** 6803–6807
39. Wang, Y., Schwedes, J. F., Parks, D., Mann, K., and Tegtmeyer, P. (1995) *Mol. Cell. Biol.* **15,** 2157–2165
40. Bakalkin, G., Yakovleva, T., Selivanova, G., Magnusson, K. P., Szekely, L., Kiseleva, E., Klein, G., Terenius, L., and Wiman, K. G. (1994) *Proc. Natl. Acad. Sci. U. S. A.* **91,** 413–417
41. Bakalkin, G., Selivanova, G., Yakovleva, T., Kiseleva, E., Kashuba, E., Magnusson, K. P., Szekely, L., Klein, G., Terenius, L., and Wiman, K. G. (1995) *Nucleic Acids Res.* **23,** 362–369
42. Fried, M., and Crothers, D. M. (1981) *Nucleic Acids Res.* **9,** 6505–6525
43. Bargonetti, J., Reynisdottir, I., Friedman, P. N., and Prives, C. (1992) *Genes & Dev.* **6,** 1886–1898
44. Bargonetti, J., Friedman, P. N., Kern, S. E., Vogelstein, B., and Prives, C. (1991) *Cell* **65,** 1083–1091
45. Kern, S. E., Kinzler, K. W., Bruskin, A., Jarosz, D., Friedman, P., Prives, C., and Vogelstein, B. (1991) *Science* **252,** 1708–1711
46. Thukral, S. K., Lu, Y., Blain, G. C., Harvey, T. S., and Jacobsen, V. L. (1995) *Mol. Cell. Biol.* **15,** 5196–5202
47. Steitz, T. A. (1990) *Q. Rev. Biophys.* **23,** 205–280
48. McNamara, P. T., Bolshoy, A., Trifonov, E. N., and Harrington, R. E. (1990) *J. Biomol. Struct. & Dyn.* **8,** 529–538
49. Satchwell, S., Drew, H. R., and Travers, A. A. (1986) *J. Mol. Biol.* **191,** 659–675
50. Bolshoy, A., McNamara, P. T., Harrington, R. E., and Trifonov, E. N. (1991) *Proc. Natl. Acad. Sci. U. S. A.* **88,** 2312–2316
51. Urpi, L., Tereshko, V., Malinina, L., HuynhDinh, T., and Subirana, J. A. (1996) *Nat. Struct. Biol.* **3,** 325–328
52. Otwinowski, Z., Schevitz, R. W., Zhang, R.-G., Lawson, C. L., Joachimiak, A., Marmorstein, R. Q., Luisi, B. F., and Sigler, P. B. (1988) *Nature* **335,** 321–329
53. Waterman, J. L. F., Shenk, J. L., and Halazonetis, T. D. (1995) *EMBO J.* **14,** 512–519
54. Wolffe, A. P. (1994) *Science* **264,** 1100–1101
55. Felsenfeld, G. (1996) *Cell* **86,** 13–19
56. Stenger, J. E., Tegtmeyer, P., Mayr, G. A., Reed, M., Wang, Y., Wang, P., Hough, P. V. C., and Mastrangelo, I. A. (1994) *EMBO J.* **13,** 6011–6020
57. Namba, H., Hara, T., Tukazaki, T., Migita, K., Ishikawa, N., Ito, K., Nagataki, S., and Yamashita, S. (1995) *Cancer Res.* **55,** 2075–2080
58. Nikolov, D. B., Chen, H., Halay, E. D., Usheva, A. A., Hisatake, K., Lee, D. K., Roeder, R. G., and Burley, S. K. (1995) *Nature* **377,** 119–128
59. Hupp, T. R., and Lane, D. P. (1994) *Curr. Biol.* **4,** 865–875
60. Pietenpol, J. A., and Vogelstein, B. (1993) *Nature* **365,** 17–18
61. Barber, A. M., and Zhurkin, V. B. (1990) *J. Biomol. Struct. & Dyn.* **8,** 213–232
62. Nagaich, A. K., Bhattacharyya, D., Brahmachari, S. K., and Bansal, M. (1994) *J. Biol. Chem.* **269,** 7824–7833
63. Shpigelman, E. S., Trifonov, E. N., and Bolshoy, A. (1993) *Cabios* **9,** 435–440
64. Ferrin, T. E., Huang, C. C., Jarvis, L. E., and Langridge, R. (1988) *J. Mol. Graphics* **6,** 13–27